Quantum-inspired information entropy in multifield turbulence

Go Yatomi[1,*] and Motoki Nakata[2,3,4]

[1]National Institute for Natural Sciences, National Institute for Fusion Science, Toki, Gifu 509-5292, Japan
[2]Faculty of Arts and Sciences, Komazawa University, Tokyo 154-8525, Japan
[3]RIKEN Center for Interdisciplinary Theoretical and Mathematical Sciences (iTHEMS), Saitama 351-0198, Japan
[4]PRESTO, Japan Science and Technology Agency, Saitama 332-0012, Japan

(Received 17 July 2024; accepted 11 April 2025; published 2 June 2025)

An information entropy for turbulence systems with multiple field quantities is formulated, as a new paradigm to explore the nonlinear dynamics and pattern formations. Combining quantum state descriptions in quantum mechanics into the turbulence field analysis, the von Neumann entropy (vNE) and the entanglement entropy (EE) are derived from a density matrix for the turbulence state in terms of the multifield singular value decomposition (MFSVD). Applying the information-theoretic entropy analyses to spatio-temporal dynamics in turbulent plasmas with phase-transition–like behavior, we discover a new nontrivial transition threshold regarding the vNE, which significantly deviates from the transition threshold of the field energy considered in the conventional approaches. These findings provide us with physically more diverse classifications of the turbulence state from the new perspective of "information", in addition to the energetics of turbulent vortices. It is also revealed that the EE for nonlinear interactions in turbulence extracts the information regarding the strength of nonlinear mode couplings and the direction of net energy transfer. A plausible application of the EE to the turbulence measurements is demonstrated, as well as the associated reconstruction technique for fluctuation fields.

DOI: 10.1103/PhysRevResearch.7.023212

I. INTRODUCTION

"Information" from a probabilistic point of view can provide us with new physical insights to extract essential properties in complicated dynamics of fields and particles. In these decades, information theory has been extensively combined into physical analyses in, e.g., quantum mechanics [1,2], the quantum gravity theory of black holes [3–5], the nonequilibrium thermodynamics [6,7], and the statistical mechanics of critical phenomena in many-body systems [8–12]. Especially, Matsueda introduced a von Neumann entropy in a classical Ising model, and discussed its scaling law around the transition and the relationship to the entanglement entropy [12]. Moreover, Pizzi and Yao formulated bipartite mutual information (MI) in classical systems by analyzing information propagation in elementary cellular automata. They demonstrated that MI is not merely a difference of entropies but a physical measure of correlations and dynamical characteristics of the system [13].

Not just in quantum mechanics, information-theoretic entropy analyses are also utilized for the studies of turbulent fluids and plasmas. One of the most standard and well-established paradigms of studying turbulence dynamics is based on the "energetics" of vortices with various scales, where the power spectrum of the turbulence energy in the wave number space is examined. Some statistically universal properties have been revealed in the formation of the power-law spectrum known as the Kolmogorov's law in homogeneous turbulence (e.g., Ref. [14]). Nevertheless, the energy cascade processes associated with significant nonlinear interactions among turbulent vortices in more general turbulence with multiple field quantities and background inhomogeneity have not fully been clarified due to their complexity and high-dimensional nature in the third-order correlation of fluctuations.

Beyond these conventional studies by turbulence energetics, there have been several recent attempts to understand turbulence in terms of entropy. For example, Falkovich *et al.* introduced a relative entropy for homogeneous steady turbulence in shell-averaged wave number space, based on multimode correlations with the Gaussian statistics [15]. Tanogami and Araki explored the nature of information flow in turbulent energy cascade processes, where the time derivative of the mutual information for the joint probability density function of the turbulence intensity at neighboring shell-averaged wave numbers is formulated [16]. Also, the von Neumann entropy for the time series data observed in laboratory plasma turbulence has been investigated [17]. It is noted that the previous works examined the information entropy concerning the integrated turbulence intensity and the temporal evolution. Thus, the inhomogeneous and/or anisotropic nature of spatial patterns of the

*Contact author: yatomi.go@nifs.ac.jp

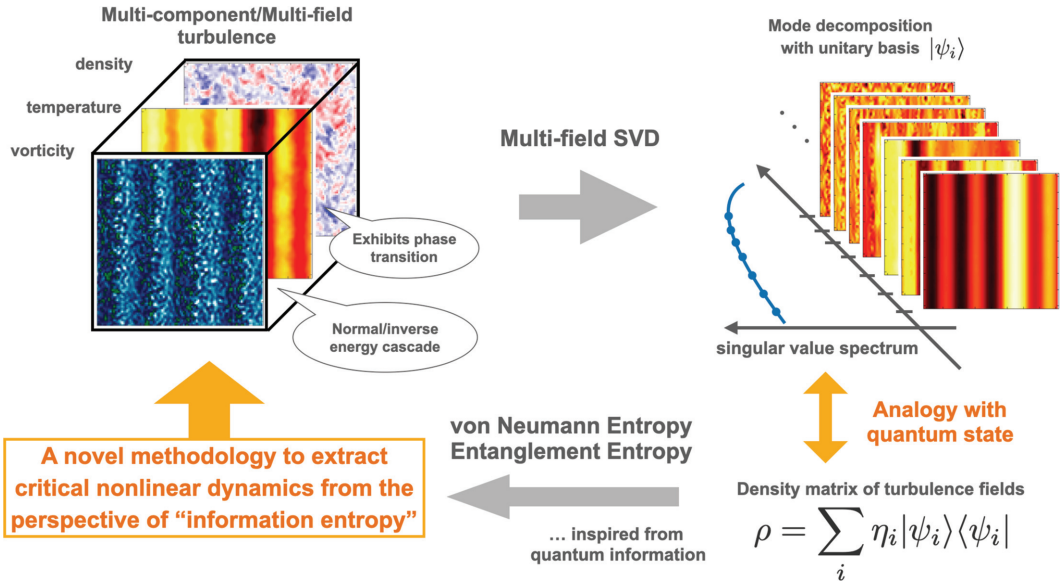

FIG. 1. The schematic diagram showing how the density matrix and the associated information entropies for multifield turbulence are constructed.

turbulence is ignored. Extensions towards the simultaneous treatment of multiple components in turbulent fields are also yet achieved.

In this work, we propose a novel information-theoretic entropy analysis for more general turbulent fields, as a new paradigm to explore the world of turbulence. The key idea is to combine quantum state arguments employing the unitary basis expansion in quantum mechanics into the turbulence field analysis. To this end, we construct a density matrix, which originally represented a quantum state, with a unitary basis reflecting spatio-temporal structures of multiple turbulent fields and coherent flow patterns. The formulation is based on our previous work of constructing "multifield" singular value decomposition (MFSVD), which is suitable for decomposing the multicomponent inhomogeneous and/or anisotropic fields [18,19]. The density matrix of turbulence enables us to derive straightforwardly the von Neumann entropy (vNE) and the entanglement entropy (EE) to quantify the coupling of subsystems, in the formal analogies of quantum mechanics and quantum information theory. Note that the EE defined here does not mean the true quantum entanglement such as Bell state, but works as a useful measure of the cross correlations in nonlinearly coupled turbulence and flows associated with the density matrix description. As will be shown later, these entropy analyses discovered a new nontrivial classification and/or description of the phase transition and nonlinear correlations in multicomponent turbulence. The key concept of this work, i.e., the integration of quantum information and turbulence dynamics, is summarized in Fig. 1.

As a representative model of a multicomponent and/or multifield turbulence system with phase-transition–like behavior, we consider the Hasegawa-Wakatani equations which will be explained in Sec. III [20,21]. The nonlinear advection in the model can produce the transition between incoherent vortices and coherent sheared-flow patterns, so-called zonal flows (ZF). The Hasegawa-Wakatani plasma turbulence is, thus, a good measure to examine our new formulations on vNE and EE of turbulence.

II. INFORMATION ENTROPIES OF TURBULENCE

A. Multifield singular value decomposition

How to construct the density matrix and associated vNE and EE for multifield turbulence is given as follows. Here, we consider two-dimensional turbulence fields (the extension to the higher dimensional case is straightforward). Let $f_p(x, y, t)$ $(p = 1, \ldots, M)$ be the p-th field component, e.g., $p = 1$ for the particle density field, $p = 2$ for the velocity field, $p = 3$ for the temperature field, etc. After discretizing on the spatial grids, the p-th field at time t is rearranged to a one-dimensional vector $\mathbf{f}_p(t) = (f_p(x_1, y_1, t), \cdots, f_p(x_{N_x}, y_1, t), \cdots, f_p(x_1, y_{N_y}, t), \cdots, f_p(x_{N_x}, y_{N_y}, t))^{\mathrm{T}}$, where N_x and N_y are the grid numbers in the x and y direction, respectively. Then, the time series of vectors for $p = 1, \ldots, M$ are combined into a $(N_x N_y) \times (N_t M)$ matrix F; $F = (\mathbf{f}_1(t_1), \cdots, \mathbf{f}_M(t_1), \cdots, \mathbf{f}_1(t_{N_t}), \cdots, \mathbf{f}_M(t_{N_t}))$, where N_t is the number of discretized time points. A schematic illustration for the construction of the matrix F is shown in Fig. 1 in Ref. [18]. Note that the matrix F simultaneously contains the spatio-temporal data for the multiple turbulence fields of interest. By applying SVD, the matrix F is decomposed by an $N \times N$ diagonal matrix of singular values $\Sigma = \mathrm{diag}(s_1, \ldots, s_N)$, an $(N_x N_y) \times N$ unitary matrix U, and a $(N_t M) \times N$ unitary matrix V, i.e., $F = U \Sigma V^{\dagger}$, where $N = \min(N_x N_y, M N_t)$ is the number of SVD modes. The mode indices are sorted in descending order of the singular values s_i. Inversely converting from the matrix form to the continuous field representation, the original p-th field quantity $f_p(x, y, t)$ is decomposed by means of the orthonormal spatial basis ψ_i and the coefficient of the

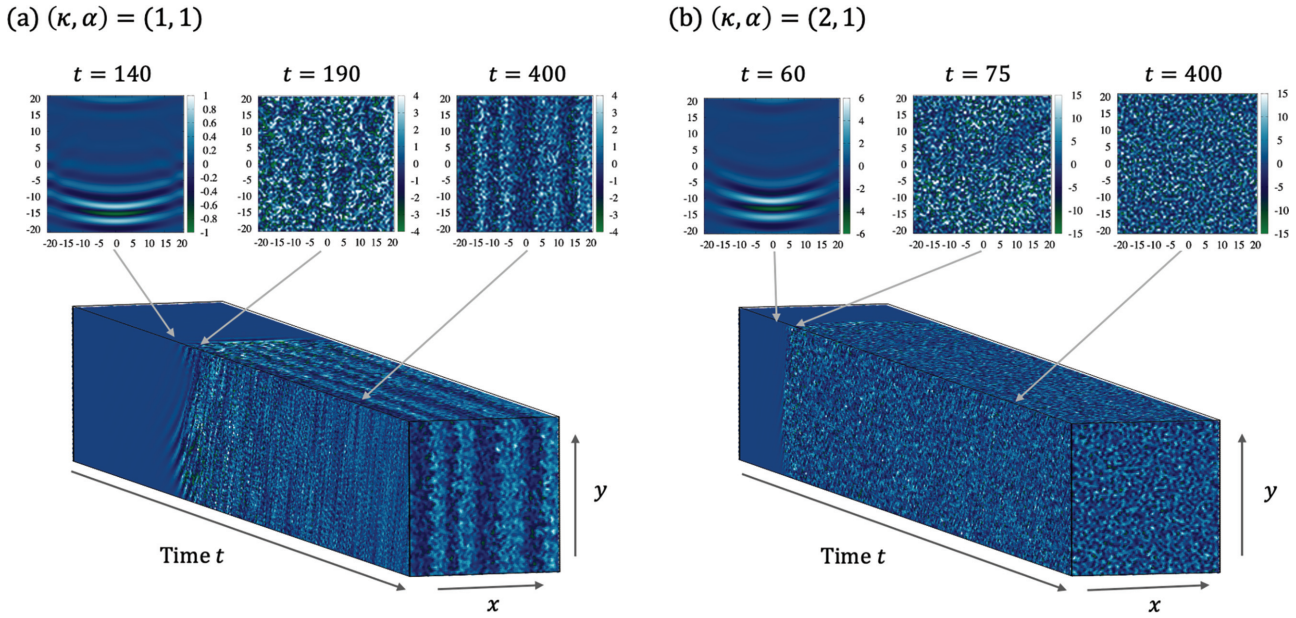

FIG. 2. The spatio-temporal evolution of the vorticity ζ in the numerical simulation of the Hasegawa-Wakatani equation. Depending on the physical parameters, turbulence dynamics bifurcates into (a) zonal-flow-dominated case $(\kappa, \alpha) = (1, 1)$ or (b) turbulence-dominated case $(\kappa, \alpha) = (2, 1)$. The snapshots of the linear growing phase (left), the saturated phase (center), and the quasisteady phase (right) are also shown.

temporal evolution $h_i^{(p)}$:

$$f_p(x, y, t) = \sum_{i=1}^{N} s_i h_i^{(p)}(t)\psi_i(x, y), \tag{1}$$

where $h_i^{(p)}$ depends on the field index p. We emphasize that s_i and ψ_i are common to the fields of interest $f_p(x, y, t)$, and thus ψ_i reflects the multifield correlation, preserving the orthonormality of the spatial structures

$$\int \mathrm{d}\mathbf{x}\psi_i\psi_j = \delta_{ij}. \tag{2}$$

It is noted that each field $f_p(x, y, t)$ is reconstructed using the common spatial basis function $\psi_i(x, y)$. In the multivariate empirical orthogonal function (MEOF) method [22], which employs singular value decomposition for meteorological analysis, the time evolution coefficients are identical for all fields by definition, while the spatial structures differ for each field. In contrast, MFSVD is designed to decompose spatially correlated nonlinear quantities, which are often integrated over space. To achieve this, we adopt a formulation distinct from that used in meteorology. Specifically, a single set of spatial basis functions $\psi_i(x, y)$ is shared across multiple fields of interest, where the label of each field is denoted by (p) in the time evolution coefficients $h_i^{(p)}(t)$. For further details of the MFSVD, including convergence properties, refer to Refs. [18,23].

B. Density matrix and information entropies

From the MFSVD, one can construct a density matrix of turbulent systems. Since the orthonormal spatial structure $\psi_i(x, y)$, which results from the unitary matrix U, can be regarded as a basis in the Hilbert space of physical field quantities in $(N_x N_y)$ dimension. Hereafter, we denote this basis using bra-ket notation such as $|\psi_i\rangle = \psi_i(x, y)$. Then, we can define a mixed state for a subsystem $X \subset \Omega = \{1, 2, \ldots, N\}$ in the whole SVD mode space Ω as follows:

$$\rho_X := \sum_{i\in X} \eta_i |\psi_i\rangle\langle\psi_i|, \tag{3}$$

$$\eta_i := \left(s_i h_i^{(p)}\right)^2 \Big/ \sum_{i\in X} \left(s_i h_i^{(p)}\right)^2, \tag{4}$$

where $\sum_{i\in X} \eta_i = 1$. Once we obtained the density matrix ρ_X, the von Neumann entropy (vNE) S_{vN}^X is derived in a similar manner to quantum systems

$$S_{\mathrm{vN}}^X := -\mathrm{Tr}(\rho_X \ln \rho_X) = -\sum_{i\in X} \eta_i \ln \eta_i. \tag{5}$$

The typical spectrum of the singular value s_i is shown in Fig. 3(a) (explained in detail later). Since $h_i^{(p)} \sim O(1)$, the vNE is approximately regarded as the Shannon entropy reflecting the broadness of the SVD mode spectrum s_i under the appropriate normalization.

The vNE is for a mixed state in the subsystem of multifield turbulence. On the other hand, we can define a compound state in two subsystems $A, B \subset \Omega$ as a tensor product form:

$$|\psi_{AB}\rangle := \sum_{i\in A}\sum_{j\in B} \sigma_{ij}|\psi_i\rangle \otimes |\psi_j\rangle, \tag{6}$$

where σ_{ij} denotes the coefficients such that $\sum_{i,j}(\sigma_{ij})^2 = 1$. The entanglement entropy (EE) of the compound state S_{EE} is derived as the vNE of the reduced density matrix

$$\rho_A = \mathrm{Tr}_B|\psi_{AB}\rangle\langle\psi_{AB}|, \tag{7}$$

$$S_{\mathrm{EE}} := -\mathrm{Tr}_A(\rho_A \ln \rho_A). \tag{8}$$

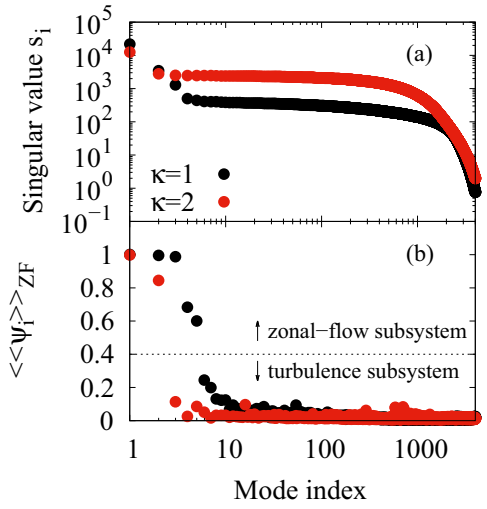

FIG. 3. The SVD spectrum of (a) the singular value s_i and (b) the zonal-flow amplitude $\langle\langle\psi_i\rangle\rangle_{\rm ZF}$. SVD modes with $\langle\langle\psi_i\rangle\rangle_{\rm ZF} > 0.4$ and $\langle\langle\psi_i\rangle\rangle_{\rm ZF} < 0.4$ constitute the zonal-flow subsystem Z and the turbulence subsystem T, respectively.

Note that, in the case of the subsystems being "entangled", the coefficients σ_{ij} must satisfy the form of $\sigma_{ij} \neq a_i b_j$. If it is expressed as a simple product form for each subsystem, i.e., $\sigma_{ij} = a_i b_j$, then the compound state is called a "separable" state, where the EE is equal to zero. The proper form of σ_{ij} is chosen to describe the nonlinear correlation of interest, as will be discussed in Eq. (13).

It should be noted that the EE defined here does not refer to quantum entanglement in the sense of a Bell state but rather serves as a novel measure of cross correlations in nonlinearly coupled classical turbulence and flows, formulated in terms of the density matrix. This definition is based on the framework where the turbulent field is decomposed into modes using the MFSVD, illustrating an analogy to the mathematical description of quantum states in Hilbert space to define the VNE and the EE.

III. MULTIFIELD TURBULENCE SYSTEM

In order to demonstrate the effectiveness of the present information entropy analysis, here we consider multicomponent plasma turbulence as a typical physical system with a complicated spatio-temporal dynamics, where the phase transition and the nonlinear correlation between multiple fields are prominent.

The waves (called the drift waves) in weakly collisional high-temperature plasmas in ambient magnetic fields can be destabilized by background inhomogeneity (in the x direction described below) of the density and/or temperature of ions and electrons. The instability growth saturates at a certain level through the nonlinear interaction of fluctuations, and then the statistically steady turbulence state is sustained. Such drift-wave turbulence in the two-dimensional plane perpendicular to the magnetic field is described by the (modified) Hasegawa-Wakatani equation in the normalized form [20,21]

$$\partial_t \zeta = \{\zeta, \phi\} + \alpha(\tilde{\phi} - \tilde{n}) - D\nabla^4 \zeta, \tag{9}$$

$$\partial_t n = \{n, \phi\} + \alpha(\tilde{\phi} - \tilde{n}) - \kappa \partial_y \phi - D\nabla^4 n, \tag{10}$$

$$\nabla^2 \phi = \zeta, \tag{11}$$

where $\nabla^2 = \partial_x^2 + \partial_y^2$, $\{A, B\} = \partial_x A \partial_y B - \partial_y A \partial_x B$. $\tilde{A} = A - \langle A \rangle$ is the nonzonal component of the quantity $A(x, y, t)$, where $\langle A \rangle = 1/L_y \int {\rm d}y A(x, y, t)$ is the zonal average in the y direction. The multiple field quantities of the electrostatic potential $\phi = \phi(x, y, t)$, the vorticity $\zeta = \zeta(x, y, t)$, and the electron density $n = n(x, y, t)$ are considered in this system. Note that the present model involves the phase-transition–like behavior between turbulence-dominated and zonal-flow-dominated states. The former is composed of incoherent vortices with various scales, whereas the latter is associated with the spontaneous generation of coherent sheared flows (will be explained below) through the turbulence cascade processes.

The turbulence dynamics bifurcates, depending on three parameters; the density gradient κ as the driving source of the linear instability, the adiabatic parameter α controlling the coupling strength of the two fields (associated with the electron motion along the magnetic field), and the dissipation coefficient D. We normalize all physical quantities to be dimensionless using the parameters of the typical scale of the turbulence or background plasmas; the time by a/C_s where a is the system length and $C_s = \sqrt{T_e/m_i}$ is the ion sound speed, the length by $\rho_s = C_s/\omega_{ci}$ where ω_{ci} is the ion gyrofrequency, the electrostatic potential ϕ by $T_e\rho_s/ea$ where T_e is the background electron temperature, and the electron density n by $n_0\rho_s/a$, where n_0 is the equilibrium electron density.

We numerically integrate the Hasegawa-Wakatani equation in the two-dimensional rectangular geometry. The periodic boundary condition is applied to both the x and y directions for simplicity. The fourth-order Runge-Kutta method is used for time integration and the Fourier spectral method is used for calculating the spatial derivatives. The grid points, the size of the simulation box, and the dissipation parameter are set as $N_x = N_y = 100$, $L_x = L_y = 2\pi/0.15 \simeq 42$, and $D = 10^{-4}$, respectively. Typically, the computation times for numerical simulation of the Hasegawa-Wakatani equation and the singular value decomposition are 0.5 CPU(48 cores) h and 1.5 CPU(48 cores) h, respectively.

The typical simulation results are shown in Figs. 2(a) and 2(b), where the zonal-flow-dominated state with $\kappa = 1$ and the turbulence-dominated state with $\kappa = 2$ are displayed. In the initial period of the simulation, the fluctuation in the drift waves linearly grows due to the primary instability [$t = 140$ in (a) and $t = 60$ in (b)]. Then, the turbulence saturates and spreads homogeneously over the entire domain [$t = 190$ in (a) and $t = 75$ in (b)]. In a reference case of $\kappa = 1$, the sheared flow with a series of antiparallel flows, which is called zonal flow (ZF), dominates the steady turbulence state [$t = 400$ in (a)]. The zonal flow is generated in the direction perpendicular to the density gradient that drives the turbulence (y direction in this case) due to the Reynolds stress through the nonlinear interactions of turbulent vortices [24]. On the other hand, in the case of relatively larger κ of $\kappa = 2$, the linear growth

rate of the drift wave turbulence increases and significantly exceeds the generation of the zonal flow due to nonlinear interactions. Then, the energy is dominated by the turbulence rather than the zonal flow, and the strongly turbulent state persists until the end of the calculation [$t = 400$ in (b)].

IV. RESULTS OF THE ENTROPY ANALYSIS

A. A new transition threshold of von Neumann entropy

In order to demonstrate the effectiveness of the present information entropy analysis, here we consider multicomponent plasma turbulence as a typical physical system with complicated spatio-temporal dynamics, where the phase transition and the nonlinear correlation between multiple fields are prominent. We carry out numerical simulations of the (modified) Hasegawa-Wakatani equation [20,21], explained in Sec. III in detail. In this numerical model, turbulence and spontaneously generated sheared flows, referred to as "zonal flow" (ZF), are described. The multiple field quantities of the electrostatic potential ϕ, the electron density n, and the vorticity ζ are considered. The quasisteady states of these fields bifurcate between the turbulence-dominated and the zonal-flow–dominated states depending on the physical parameters of the density gradient κ, the adiabatic parameter α, and the dissipation coefficient D as will explained in Fig. 2.

Since the spontaneous zonal-flow formation occurs by the nonlinear interactions between ϕ and ζ, the MFSVD for these two fields is applied to the simulation data for the quasisteady state. The resultant singular value spectra for $\kappa = 1$ and 2 are shown in Fig. 3(a). Then we divide the SVD modes into two subsystems, i.e., the zonal-flow subsystem Z and the turbulence subsystem T, according to a threshold of the relative zonal-flow amplitude of the mode $\langle\langle\psi_i\rangle\rangle_{\rm ZF}$; $Z = \{i\,|\langle\langle\psi_i\rangle\rangle_{\rm ZF} > 0.4\}$ and $T = \{i\,|\langle\langle\psi_i\rangle\rangle_{\rm ZF} < 0.4\}$, where $\langle\langle\psi_i\rangle\rangle_{\rm ZF} = \int dx(\int dy\,\psi_i)^2/\int dxdy\,(\psi_i)^2$. The SVD spectra of $\langle\langle\psi_i\rangle\rangle_{\rm ZF}$ are shown in Fig. 3(b). The zonal-flow subsystem Z exists in the first few modes, modes, i.e., the first five modes for $\kappa = 1$ in Fig. 3(b), and the turbulence subsystem T consists of the later thousands of modes , i.e., all other modes for $\kappa = 1$ in Fig. 3(b). By doing this, one can examine vNE for the zonal flow and the ambient turbulence separately.

Figure 4(a) shows the κ dependence of the relative energy ratio of the zonal flow, indicating a clear transition at $\kappa \simeq 1.5$, defined by the point where $E_{\rm ZF}/E_{\rm T} = 0.5$, where $E_{\rm ZF} = \int d\mathbf{x}(-\langle\phi\rangle\langle\zeta\rangle)$ is the zonal-flow energy and $E_{\rm T} = \int d\mathbf{x}(-\phi\zeta)$ is the total energy, where $\langle A\rangle = 1/L_y\int dyA(x, y, t)$ is the zonal average in the y direction. This is the conventional way of identifying the phase transition between the zonal-flow-dominated and turbulence-dominated states (e.g., Ref. [21]). For fixed $\alpha = 1$, the zonal flow is strongly generated in the region of $\kappa < 1.5$ with the moderate linear growth rate of the turbulent fluctuations, while the zonal flow is suppressed in the large κ region where the ambient turbulence strongly grows.

The κ dependence of vNE for the turbulence subsystem $S^T_{\rm vN}$ and the zonal-flow subsystem $S^Z_{\rm vN}$ are shown in Fig. 4(b). $S^T_{\rm vN}$ is considerably larger than $S^Z_{\rm vN}$ in the whole region of κ. This is because the zonal-flow subsystem consists of only several SVD modes as shown in Fig. 3(b), while the turbulence subsystem is composed of a number of SVD modes with a broader distribution. In contrast to the conventional energy-ratio argument, another kind of phase transition with respect to vNE is discovered in the turbulence subsystem, where the transition threshold, $\kappa \simeq 0.7$, is clearly smaller than that in the energy ratio, $\kappa \simeq 1.5$. Here, the threshold of $S^T_{\rm vN}$ is defined by the κ value where the $S^T_{\rm vN}$ bisects the maximum and the minimum values with α fixed. It is also noted that $S^Z_{\rm vN}$ captures the energy-ratio transitions as well. Indeed, for $\kappa < 1.5$, nearly zero value of $S^Z_{\rm vN}$ is associated with a significantly shrunk SVD mode spectrum. Around the critical value in the energy ratio, $\kappa \simeq 1.5$, $S^Z_{\rm vN}$ increases because of the broadening of the SVD mode spectrum, which is physically interpreted as a perturbed state with the various scales of zonal flows. In the large κ limit where $S^Z_{\rm vN}$ decays, the number of the zonal-flow modes quickly decreases.

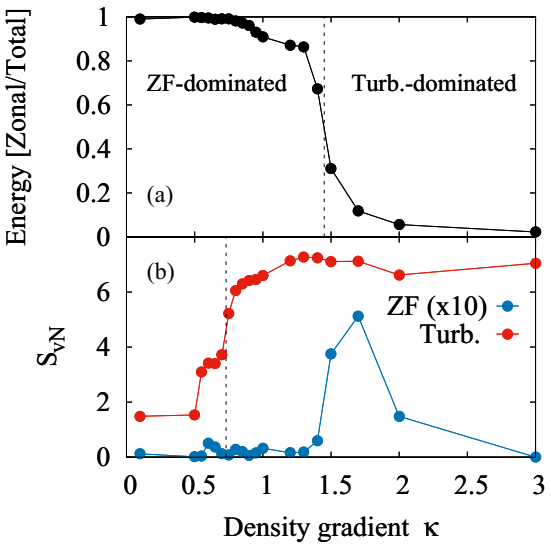

FIG. 4. (a) κ dependence of the relative zonal-flow energy ratio, and (b) the von Neumann entropy of the zonal-flow subsystem (blue) and the turbulence subsystem (red).

Based on these findings from quantum-inspired information entropy analyses, we can identify the new classification of states in plasma turbulence, i.e., [State i] zonal-flow-dominated state with small $S^T_{\rm vN}$, [State ii] zonal-flow dominated state with large $S^T_{\rm vN}$, and [State iii] turbulence-dominated state with large $S^T_{\rm vN}$. These are summarized in Table I, and the typical spatial structures for each case will be discussed in Fig. 6.

Figure 5 shows the contour plots of the vNE for turbulence and zonal-flow subsystems in the κ-α parameter space. The

TABLE I. The classification of quasisteady state based on the energy ratio and the von Neumann entropy.

	$E_{\rm ZF}/E_{\rm T}$	$S^T_{\rm vN}$	$S^Z_{\rm vN}$
[State i]	large	small	small
[State ii]	large	large	small
[State iii]	small	large	large

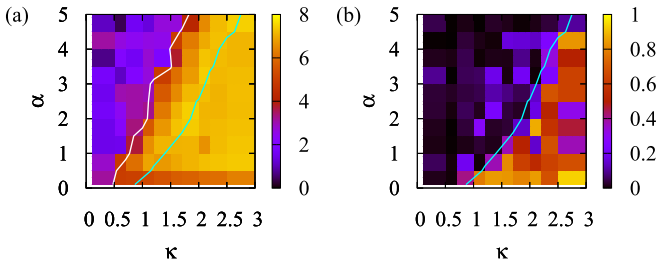

FIG. 5. The contours of the von Neumann entropy of (a) the turbulence subsystem $S^T_{\rm vN}$ and (b) the zonal-flow subsystem $S^Z_{\rm vN}$ in the κ-α space. The white and cyan curves show the boundary of $S^T_{\rm vN}$ and the relative energy ratio where $E_{\rm ZF}/E_{\rm T} = 0.5$, respectively. The separation of the boundaries of $E_{\rm ZF}/E_{\rm T}$ (cyan) and $S^T_{\rm vN}$ (white) indicates the nontrivial classification of turbulent state by the vNE. The boundary of $S^Z_{\rm vN}$ also captures the conventional energy boundary.

cyan curves represent the transition threshold in the conventional energy ratio, where the critical value of $E_{\rm ZF}/E_{\rm T} = 0.5$ is considered. The entropy transition boundary for $S^T_{\rm vN}$, shown by the white curve in Fig. 5(a), clearly deviates from the energy transition boundary. Thus, it is repeatedly noted that there exists a novel classification of the quasi-steady states from the information point of view. On the other hand, the entropy transition boundary of $S^Z_{\rm vN}$ shown in Fig. 5(b) reasonably coincides with the energy transition boundary, as explained in Fig. 4(b).

B. Physical interpretation of the information entropy boundary

The contour of the spatial structure of each subsystem $\phi_Z(x,y) = \sum_{i\in Z} s_i h_i^{(\phi)} \psi_i(x,y)$ and $\phi_T(x,y) = \sum_{i\in T} s_i h_i^{(\phi)} \psi_i(x,y)$ is shown in Fig. 6. The zonal-flow velocity profile $U(x) = \partial_x \langle \phi \rangle$ is also displayed. The color bars for contours ϕ_T and ϕ_Z and the y axis of the zonal-flow velocity U are normalized to emphasize the spatial patterns. The actual ratio for the amplitude of the two subsystems is shown in Fig. 4(b). The two panels on the left correspond to [State i], the two panels in the middle correspond to [State ii], and the two panels on the right correspond to [State iii] as discussed in Fig. 4. For the turbulence subsystem, the vortex streets trapped in the crest of the zonal flow [25,26] in [State i]. Note that the transition of the information entropy for nonzonal turbulent fluctuations occurs even in the zonal-flow–dominated state and has never been captured by the conventional energetics arguments. Although the trapping of turbulent vortices by the zonal flow is recognized in previous works [27,28], the bifurcation of the trapped and the untrapped states is newly revealed quantitatively by the present information entropy analyses.

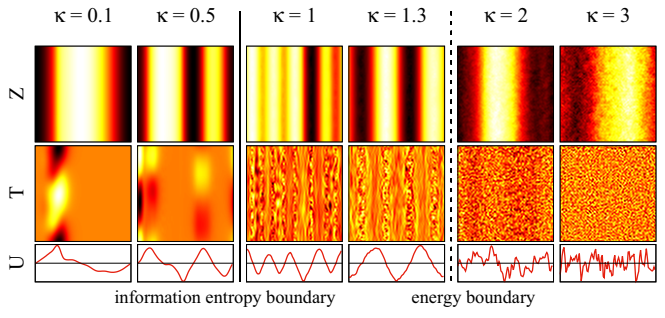

FIG. 6. The contour of the spatial structure of each subsystem $\phi_T(x,y)$ and $\phi_Z(x,y)$ and the zonal-flow velocity U (with black lines representing $U = 0$) for several κ values. α is fixed to 1 in all cases. The color scales for contours ϕ_T and ϕ_Z and the y axis of the zonal-flow velocity U are normalized. Below the information entropy boundary, the turbulent vortices are trapped in the crest of zonal flow velocity U. On the other hand, the trapping becomes less significant above the information entropy boundary despite the presence of the strong zonal flow.

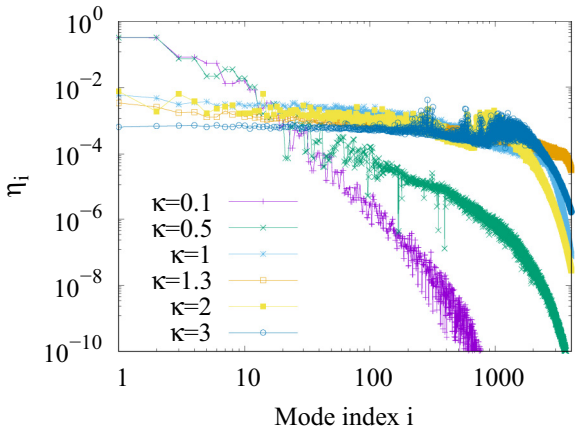

FIG. 7. The time-averaged spectra of η_i for $\kappa = \{0.1, 0.5, 1, 1.3, 2, 3\}$, where $\alpha = 1$ in all cases.

The bifurcation of the vNE is directly observed from the spectra of η_i in Eq. (4) shown in Fig. 7. In [State i] with $\kappa = 0.1$ and 0.5, the spectra are dominated by first several modes corresponding to trapped large-scale vortices, and then the amplitude for latter modes significantly decays. These peaked spectra correspond to relatively smaller values of information entropy. On the other hand, in [State ii] and [State iii] with the larger entropies, the broader spectra of η_i indicate comparable contributions of the amplitude up to approximately 1000 modes, corresponding to the co-existence of multiscale vortices.

Detailed variations near the information entropy transition point are shown in Fig. 8. As shown in panel (a), the transition occurs smoothly, including intermediate states where $S^T_{\rm vN}$ is almost constant. In other words, this transition is considered to be a kind of second- or higher-order phase transition, although the relative energy ratio shows the first-order–like transition within this resolution of the simulation. The continuous change in entropy can also be read from the change in the spectrum of e shown in panel (b). In the intermediate case of the transition with $0.55 \leqslant \kappa \leqslant 0.8$, the contribution of the first few modes representing trapped vortex streets decreases, while the contribution of the 100 to 1000 modes representing homogeneous turbulence increases. This is confirmed by the contours of the spatial structure of the turbulent subsystem $\phi_T(x,y)$ in the intermediate case with $\kappa = 0.7$ shown in panel (c). One can observe not only trapped vortex streets but also smaller-scale turbulent eddies in the x region between vortex streets.

Explicating the meaning of vNE, it is useful to examine the Fourier wave number spectra between the information entropy

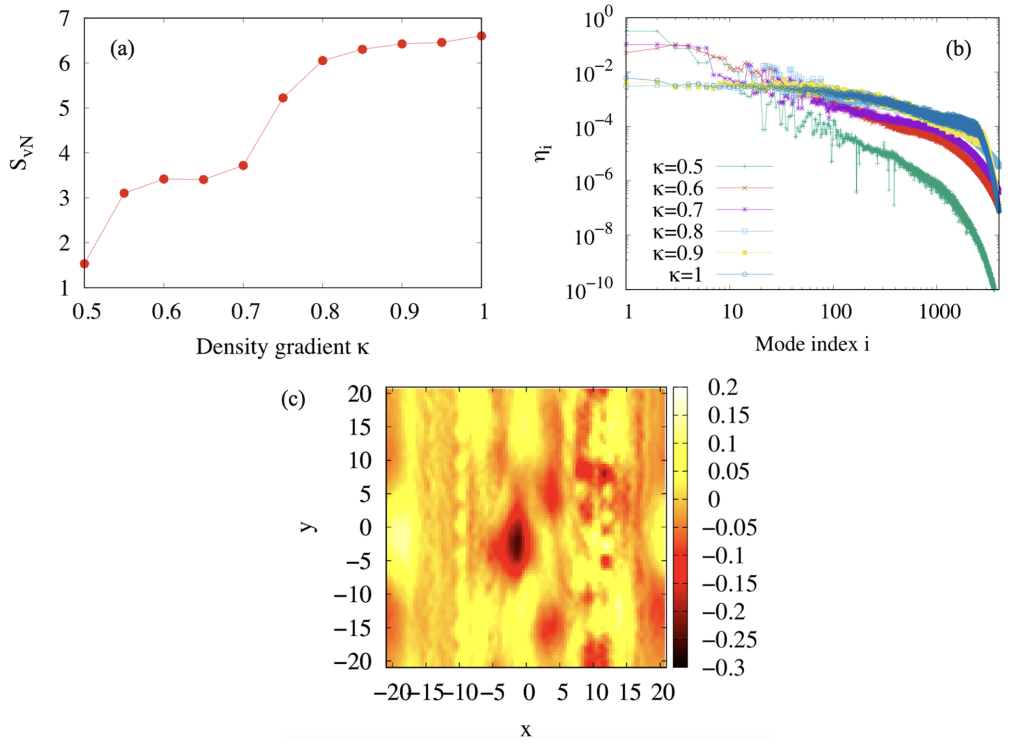

FIG. 8. Detailed plots of the von Neumann entropy S^T_{vN} near the information entropy transition point. (a) κ dependence of the von Neumann entropy of the turbulence subsystem S^T_{vN}, (b) the time-averaged spectra of η_i for $\kappa = \{0.5, 0.6, 0.7, 0.8, 0.9, 1\}$, (c) the contour of the spatial structure of the turbulence subsystem $\phi_T(x, y)$ in the typical intermediate case with $\kappa = 0.6$, where $\alpha = 1$ in all cases.

boundary. Figure 9 shows the time-averaged Fourier spectrum of the electrostatic potential ϕ_{k_x,k_y}, where the boundary between zonal ($k_y = 0$) and turbulence ($k_y > 0$) modes is indicated by the cyan line. One can see that when κ exceeds the information entropy boundary of $\kappa \simeq 0.7$, the spectral shapes for turbulence modes are expanded to the high-wave number region. It should be noted that the multidimensional investigations in the whole wave number space are needed to identify such transition by the Fourier decomposition approach even though one can recognize the spectral deformation by direct visualizations. Also, the transition at $\kappa \simeq 0.7$, as shown in Fig. 4(a), is no longer captured by the conventional energetics argument that evaluates the ratio of the spectral integral for zonal and turbulence modes in the Fourier wave number space. On the other hand, the vNE constructed in this study can quantify the change of spectral shape by only a single scalar value. It is also remarkable that the combined argument with individual vNE for the zonal and turbulence modes can capture the energy boundary as well [see Fig. 4(b)]. This highlights the beneficial characteristics of the vNE from a turbulence analysis point of view. The information entropy analysis is straightforwardly applicable even in non-uniform turbulence systems where the Fourier decomposition is invalid.

The physical mechanism of the novel bifurcation discovered by the vNE is understood as follows. Even in

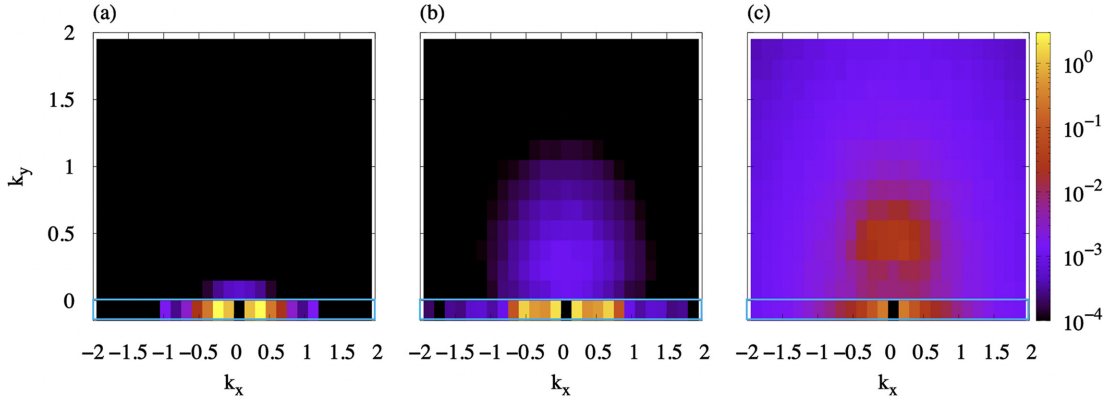

FIG. 9. The contours of the time-averaged Fourier spectra of ϕ_{k_x,k_y} in the cases of (a) $\kappa = 0.5$, (b) $\kappa = 1$, and (c) $\kappa = 3$, where $\alpha = 1$ in all cases. The grids of the zonal modes ($k_y = 0$) are encircled by cyan squares.

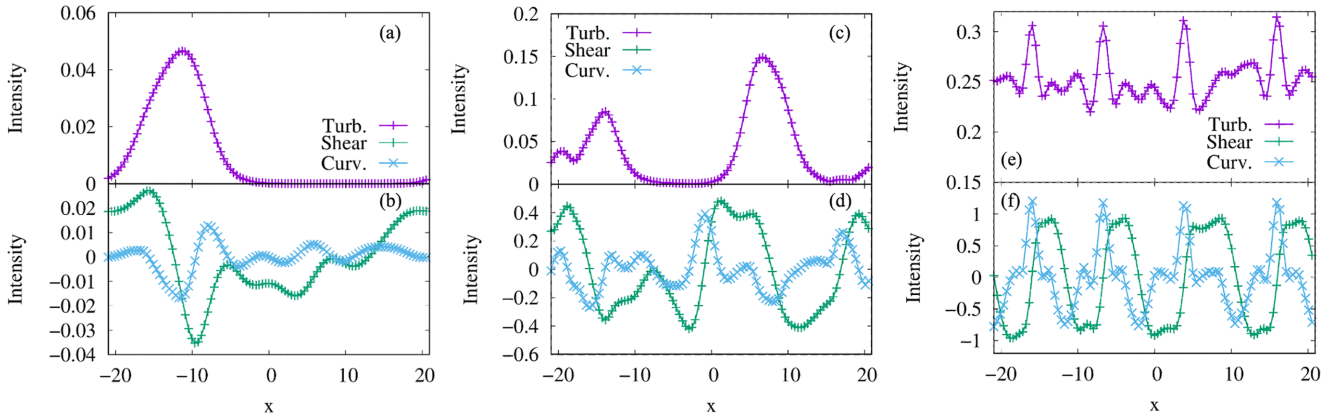

FIG. 10. The time average of (a),(c),(e) the y-averaged turbulence intensity, (b),(d),(f) the shear and the curvature of the zonal flow. (a),(b) show the case of $\kappa = 0.1$, (c),(d) show $\kappa = 0.5$, and (e),(f) show $\kappa = 1$, where $\alpha = 1$ in all cases.

the zonal-flow-dominated state, several destabilization mechanisms to drive turbulent vortices through the nonlinear interactions with the zonal flow $U(x)$ have been revealed. Particularly important factors are known as the shearing effect $\partial_x U(x)$ [24,29] and the curvature effect $\partial_x^2 U(x)$ [27,30]. Then, we investigate the correlation between the turbulence intensity, the shear, and the curvature. Figure 10 compares the time-averaged spatial patterns of the turbulence intensity averaged in the y direction, the zonal-flow shear, and the zonal-flow curvature around the information entropy boundary. For [State i] with $\kappa = 0.1$ [panels (a) and (b)] and $\kappa = 0.5$ [panels (c) and (d)], one can see that the region where the turbulence is locally trapped corresponds to the region with the negative curvature. On the other hand, for [State ii] with $\kappa = 1$ shown in Figs. 10(e) and 10(f), the maxima of turbulence intensity coincide with regions of the positive curvature. Moreover, the turbulence intensity is broadened over the x region where the zonal-flow shear is significant. This suggests that the predominant contribution of driving mechanisms for the zonal-flow instabilities and the resulting vortex trapping changes between the information entropy boundary. The intensity balance of zonal-flow shear and the negative/positive curvature is a key factor to characterize the qualitative difference in the spatial patterns, which is reflected in the vNE.

C. Entanglement entropy of nonlinear interaction

In both the Fourier wave number space and SVD mode space, the nonlinear interactions in the turbulence system are described by the triad energy transfer $\mathcal{J}_l^{i,j}$ [18,31]. In the present formulation using the MFSVD, it is expressed as

$$\begin{aligned}\mathcal{J}_l^{i,j} &:= \frac{1}{2}\int \mathrm{d}\mathbf{x}\, \phi_l(\{\phi_i, \zeta_j\} + \{\phi_j, \zeta_i\}) \\ &= \frac{1}{2} s_i s_j s_l h_l^{(\phi)} \left(h_i^{(\phi)} h_j^{(\zeta)} - h_j^{(\phi)} h_i^{(\zeta)}\right) \int \mathrm{d}\mathbf{x}\, \psi_l \{\psi_i, \psi_j\}.\end{aligned} \tag{12}$$

Here, (i, j, l) means the SVD mode indices. Note that $\mathcal{J}_l^{i,j} = \mathcal{J}_l^{j,i}$ and $\mathcal{J}_l^{i,j} + \mathcal{J}_j^{l,i} + \mathcal{J}_i^{j,l} = 0$.

The triad energy transfer is a multivariable function that depends on three mode indices (i, j, l) and the time t. In particular, the mode index in the Fourier decomposition is a wave number that is itself a multidimensional quantity. Therefore, the triad energy transfer can be a seven-variable function in two-dimensional fluid or a ten-variable function in three-dimensional fluid. Then, it is quite difficult to analyze simultaneously the temporal evolution and the mode-space structures in terms of the Fourier decomposition. In the MFSVD, however, the dimension of $\mathcal{J}_l^{i,j}$ is reduced since the mode index in the SVD is just an integer. Then, it is possible to visualize and analyze the time-averaged mode-space structure of $\mathcal{J}_l^{i,j}$ as shown in Fig. 11. Here, the contour of $\mathcal{J}_l^{i,j}$ in (a) the zonal-flow-dominated state and (b) the turbulence-dominated state are compared. It is found that the nonlinear interaction is concentrated on several modes in the zonal-flow-dominated state, while it is widely distributed in many modes in the turbulence-dominated state. Although this type of analysis renders substantial understandings of nonlinear interactions in turbulent systems, it is limited to the time average of $\mathcal{J}_l^{i,j}$, and the temporal behavior is completely ignored. Then, we propose the EE as the dimensionality-reduced $\mathcal{J}_l^{i,j}$ retaining the structural information on the SVD mode space, rather than a simple average of variables. Since the triad energy transfer $\mathcal{J}_l^{i,j}$ indicates the negative and positive values depending on the direction of energy flow, the exponential form is appropriate to the condition of $\sum_{i,j}(\sigma_{ij})^2 = 1$:

$$\sigma_{ij}^{\pm} := C \exp\left(\pm \mathcal{J}_l^{i,j}\right), \tag{13}$$

where $C = \{\sum_{i,j} \exp(\pm \mathcal{J}_l^{i,j})\}^{-\frac{1}{2}}$ and l is arbitrary but fixed here. Two expressions of the EE are then derived from Eq. (8); S_{EE}^{+} for σ_{ij}^{+} and S_{EE}^{-} for σ_{ij}^{-}. We choose this form of the coefficients in order not to make the state separable and to distinguish between inflows (S_{EE}^{+}) and outflows (S_{EE}^{-}) of the energy transfer. In this formulation, the EE is just a real scalar value that extracts the nonlinear coupling of turbulence fields as the information quantity. The EE enables the dimensionality reduction of the original $\mathcal{J}_l^{i,j}$, still retaining the information on the direction of the transfer and the structures in the mode space, which is lost by the simple summation by the indices (or wave numbers). Similar to quantum mechanics, a large value of the EE means that only several limited modes are strongly coupled to drive energy transfer via the zonal mode.

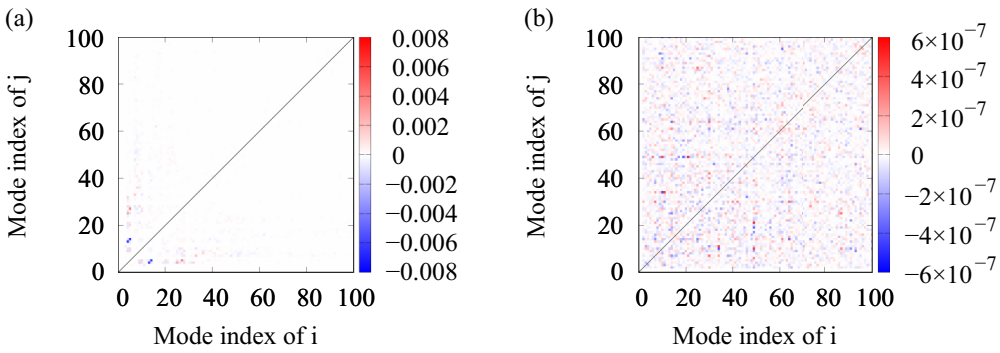

FIG. 11. The contour of the time-averaged triad energy transfer $\mathcal{J}_l^{i,j}$ in the SVD mode space. (a) shows the zonal-flow-dominated state with $(\kappa, \alpha) = (1, 3)$ and (b) shows the turbulence-dominated state with $(\kappa, \alpha) = (3, 1)$. The index l is fixed to 1 in both cases.

Figure 12 shows the comparison of the temporal evolution of the field energy and the EE in the case of $(\kappa, \alpha) = (1, 3)$. In all parameter regions in this work, the SVD mode of $l = 1$ is the mode that represents the spatial structure of the zonal flow. Then, the subscript l in $\mathcal{J}_l^{i,j}$ is fixed to the zonal-flow mode $l = 1$ to look into the nonlinear energy transfer mediated by the zonal flow. As shown in panel (a), the field energy of the zonal flow changes in the slow time scale. However, the EE shown in panel (b) oscillates in a much smaller time scale compared to the energy variation. Then, it is found that the slow variation of the field energy results from the accumulation of many instantaneous nonlinear interactions.

While both expressions of the EE $S_{\rm EE}^+$ and $S_{\rm EE}^-$ have similar values during periods of increasing and decreasing energy, the difference between them is shown in Fig. 12(c) as the temporal evolution of the probability density function (PDF) of $S_{\rm EE}^+ - S_{\rm EE}^-$. During the field energy decaying ($1350 < t < 1400$), $S_{\rm EE}^-$ is relatively larger than $S_{\rm EE}^+$, and the peak value of the PDF moves to the negative region of $S_{\rm EE}^+ - S_{\rm EE}^-$. Then, $S_{\rm EE}^+$ becomes dominant over $S_{\rm EE}^-$ and the PDF peaks at the positive region when the field energy is growing ($1400 < t < 1470$). When the growth rate of the ZF energy settles down at $t \simeq 1480$, the peak of the PDF tends to be negative again, implying the saturation of growth.

Figure 13 shows the case where the turbulence dominates and the field energy is nearly steady $(\kappa, \alpha) = (3, 1)$. The EE has a finite value and rapidly oscillates like the case of $(\kappa, \alpha) = (1, 3)$. However, $S_{\rm EE}^+$ and $S_{\rm EE}^-$ balance and the PDF peaks at 0, corresponding to the fact that the energy transfer is statistically constant in both the positive and negative directions. Therefore, the EE for the turbulence system provides information on not only the strength of the nonlinear coupling

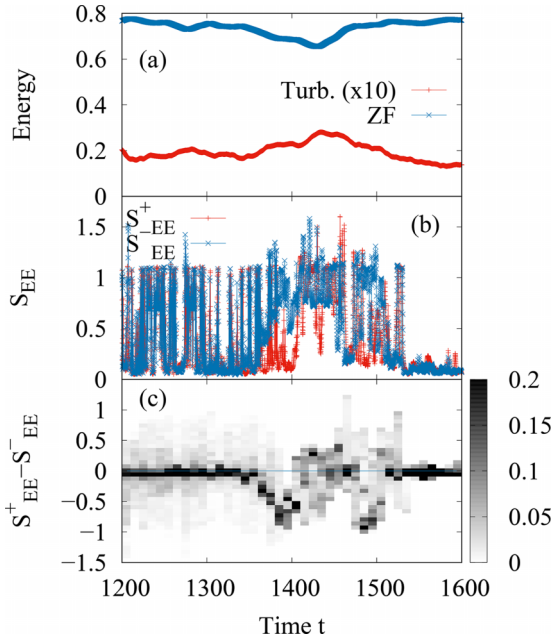

FIG. 12. The temporal evolution of (a) the field energy of the turbulence (red) and the zonal flow (blue), (b) the entanglement entropy $S_{\rm EE}^+$ (red) and $S_{\rm EE}^-$, and (c) the probability density function (shown as the color bar) of the difference of the entanglement entropy $S_{\rm EE}^+ - S_{\rm EE}^-$ in the case of $(\kappa, \alpha) = (1, 3)$.

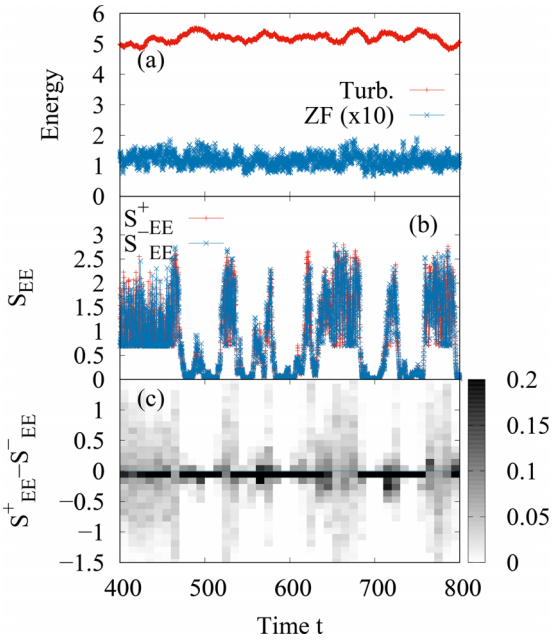

FIG. 13. The temporal evolution of (a) the field energy of the turbulence (red) and the zonal flow (blue), (b) the entanglement entropy $S_{\rm EE}^+$ (red) and $S_{\rm EE}^-$, and (c) the probability density function (shown as the color bar) of the difference of the entanglement entropy $S_{\rm EE}^+ - S_{\rm EE}^-$ in the case of $(\kappa, \alpha) = (3, 1)$.

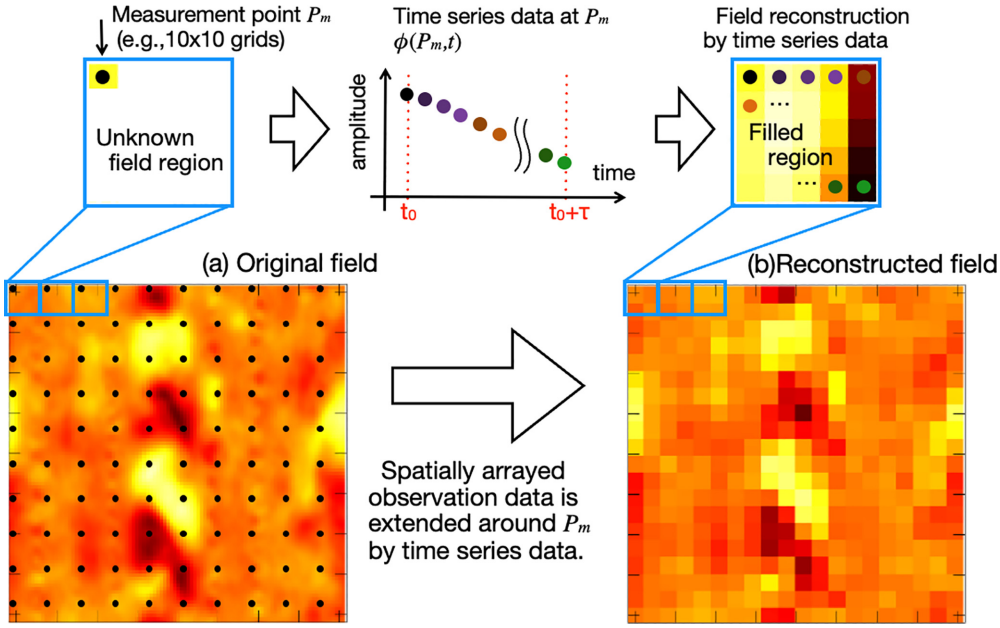

FIG. 14. The snapshot of ϕ in (a) original and (b) reconstructed data with $n_d = 20$ at $t = 1200$ in the case of $(\kappa, \alpha) = (1, 3)$. The procedure of how to reconstruct the coarse-grained field from the spatially arrayed observation data is also displayed.

but also the direction of the energy transfer. In other words, the present EE is a scalar quantity representing the information flow in the nonlinear interaction, but keeping the spatial structures in the unitary basis $\psi(x, y)$. Note that similar analyses to examine directly $\mathcal{J}_l^{i,j}$ including their temporal dynamics are often difficult in the conventional mode-by-mode approach.

D. Application of the entanglement entropy

As is demonstrated above, the EE provides us with a new perspective of turbulence nonlinearities from an information-theoretic point of view. In addition to such conceptual extensions, the EE involves important applications to the practical problems in turbulent plasmas, which are typical systems of multifield turbulence. Here, we present a plausible application of the EE to fluctuation field measurements, which are important issues in laboratory plasma experiments and astronomical observations. As will be shown below, the EE works as a good measure to determine the necessary grid points of spatio-temporal observation while keeping the information of nonlinear interactions.

In magnetically confined plasma experiments, the spatial patterns of the density or potential fluctuations in turbulence are often measured by an array of detectors in the order of several tens [32], where each line of sight corresponds to the discrete spatial point in the fluctuation field to be observed. Many efforts have been devoted to upgrading the spatial resolution by increasing the grid points of the detector array to measure the finer- and faster-scale structures. Although the spatio-temporal resolution cannot be large enough because of the size of the detectors and/or the signal-to-noise ratio, it is easier to obtain the data for a sufficiently long duration. The EE with an associated reconstruction technique provides us with a novel guideline to determine how many measurement points are necessary to capture the nonlinear interactions in the turbulent fluctuations.

To demonstrate the usefulness of the EE for turbulence measurement, we imitate an experimental situation by a numerical simulation, as shown in Fig. 14. Suppose the black dots in the original fluctuation field (left panel in the figure) to be the detection points $P_{\rm m}$, then one can only obtain the fluctuation data at those points in the measurement situation. Here, such spatially arrayed observation data is extended around $P_{\rm m}$ by using the time series data with an interval of τ, which is sufficiently smaller than the turbulence time scale, to reconstruct the global spatial profile of the fluctuation as the $N \times N$ matrix data. First, let $n_d \times n_d$ be the number of detector array, then the original $N_f \times N_f$ fluctuation field at time t_0 is divided into $n_d \times n_d$ blocks of $(N_f/n_d) \times (N_f/n_d)$ matrices. The position of each measurement point is regarded as the representative position in each block, i.e., $(x_{mN_f/n_d+1}, y_{mN_f/n_d+1})$ where $m = 0, \ldots, n_d - 1$.

Secondly, at each representative point, the time series of n_d^2 in $[t_0, t_0 + n_d^2 \Delta t)$ at $(x_{mN_f/n_d+1}, y_{mN_f/n_d+1})$ are distributed to the other spatial positions to fill up the undetected region. Then, one can obtain the reconstructed fluctuation field shown in Fig. 14(b), where the spatial patterns are somewhat coarse-grained in comparison to the original field. Once the fluctuation field is reconstructed by the above technique, the vNE and the EE are straightforwardly calculated by using the MFSVD.

We investigated the dependence of the EE on the measurement points or the division number n_d as shown in Fig. 15. In the case of $n_d = 5$, it shows rapid oscillations as in the original data that indicate the instantaneous nonlinear energy transfer between turbulence and zonal flows. However, the time evolutions are almost identical, and the original behavior for the PDF of $S_{\rm EE}^{+} - S_{\rm EE}^{-}$ is no longer reproduced. As n_d increases, e.g., $n_d = 20$ and 50, the behavior of the EE approaches to

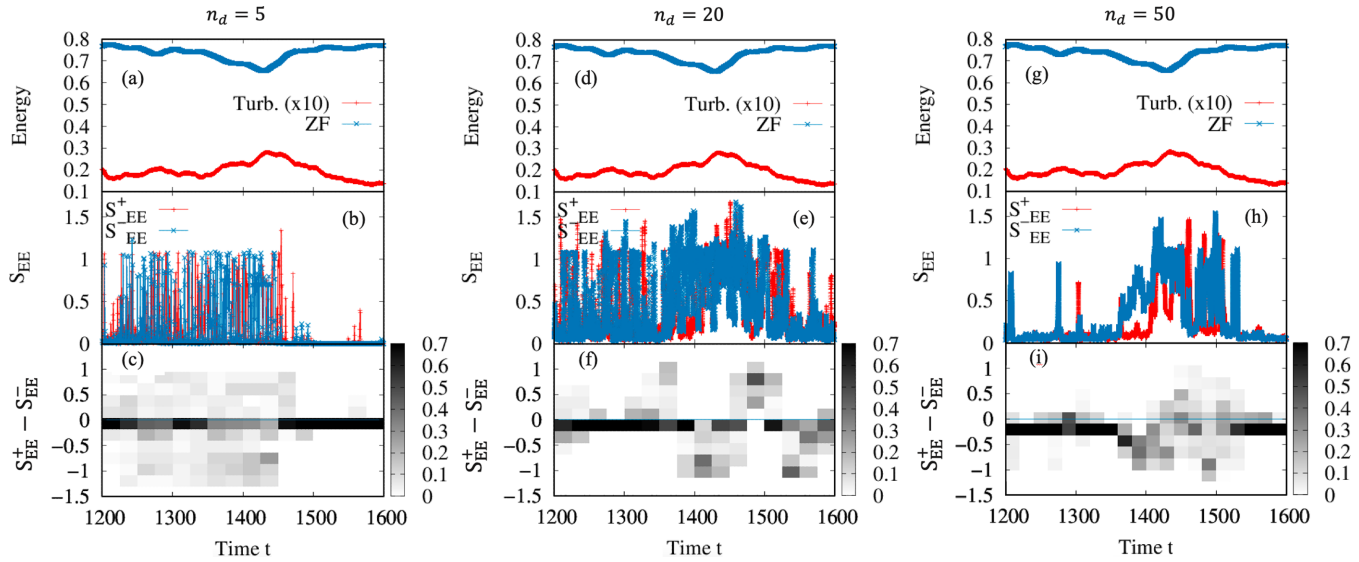

FIG. 15. The temporal evolution of (a),(d),(g) the field energy of the turbulence (red) and the zonal flow (blue). (b),(e),(h) the entanglement entropy $S^+_{\rm EE}$ (red) and $S^-_{\rm EE}$. (c),(f),(i) the probability density function of the difference of the entanglement entropy $S^+_{\rm EE} - S^-_{\rm EE}$ in the case of $(\kappa, \alpha) = (1, 3)$. The left panels (a)–(c) show the case of the division number $n_d = 5$, and the center (d)–(f) and right (g)–(i) panels indicate the case for $n_d = 20$ and $n_d = 50$, respectively.

the original data, i.e., the PDF of $S^+_{\rm EE} - S^-_{\rm EE}$ tends to negative when the ZF energy decreases and vice versa, and the rapid oscillation of the EE becomes less significant after the gradual recovery of the zonal-flow energy for $t > 1550$.

The clarification of n_d dependence implies that the EE works as a good measure for the reproducibility of nonlinear interactions even in the limited resolution of fluctuation field measurements. In addition, the similar application of the EE can be useful for the information reduction from large-scale turbulence simulation and observation data, but keeping the crucial nonlinear nature. The application of the information entropy to detect the optimal spatio-temporal resolution, which tends to be ambiguous, enables us to expand a new aspect beyond the conventional spectral or energetics approach relying on Fourier decomposition.

V. SUMMARY

In this work, we formulate the quantum-inspired information entropy of multifield turbulence. Using the multifield singular value decomposition (MFSVD), the density matrix for the turbulence state is constructed. Then, the von Neumann entropy (vNE) and the entanglement entropy (EE) are derived. As a result, we discover a novel transition of the turbulence structure based on the information entropy, which cannot be seen by the conventional energy argument. Furthermore, the present EE can provide new insights into nonlinear interactions in turbulence. It should be emphasized that the proposed formulation can be applied to any other kinds of turbulent fields and related physical systems with nonlinear correlations, beyond the present turbulent plasmas. We also demonstrated a plausible application of the EE to the turbulence measurements, as well as the associated reconstruction technique for the fluctuation fields. Practical applications of the vNE and the EE as novel turbulence measurement principles will be addressed in realistic experiments and observations.

ACKNOWLEDGMENTS

We thank Makoto Sasaki and Masayuki Yokoyama for the helpful discussions. Numerical computations are performed on the NIFS Plasma Simulator. This work was supported in part by JST, the establishment of university fellowships towards the creation of science technology innovation, Grant No. JPMJFS2136, in part by JST, PRESTO Grant No. JPMJPR21O7, and in part by the NIFS collaborative Research programs (NIFS23KIST039, NIFS23KIST044).

[1] V. Vedral, M. B. Plenio, M. A. Rippin, and P. L. Knight, Quantifying entanglement, Phys. Rev. Lett. **78**, 2275 (1997).
[2] R. Horodecki, P. Horodecki, M. Horodecki, and K. Horodecki, Quantum entanglement, Rev. Mod. Phys. **81**, 865 (2009).
[3] J. D. Bekenstein, Black holes and entropy, Phys. Rev. D **7**, 2333 (1973).
[4] S. Das and S. Shankaranarayanan, Entanglement as a source of black hole entropy, J. Phys.: Conf. Ser. **68**, 012015 (2007).
[5] E. D. Belokolos and M. V. Teslyk, Scalar field entanglement entropy of a Schwarzschild black hole from the Schmidt decomposition viewpoint, Class. Quantum Grav. **26**, 235008 (2009).
[6] C. H. Bennett, Demons, Engines and the second law, Sci. Am. **257**, 108 (1987).
[7] T. Sagawa and M. Ueda, Second law of thermodynamics with discrete quantum feedback control, Phys. Rev. Lett. **100**, 080403 (2008).

[8] C. Holzhey, F. Larsen, and F. Wilczek, Geometric and renormalized entropy in conformal field theory, Nucl. Phys. B **424**, 443 (1994).

[9] G. Vidal, J. I. Latorre, E. Rico, and A. Kitaev, Entanglement in quantum critical phenomena, Phys. Rev. Lett. **90**, 227902 (2003).

[10] S. Dong, E. Fradkin, R. G. Leigh, and S. Nowling, Topological entanglement entropy in Chern-Simons theories and quantum Hall fluids, J. High Energy Phys. 05 (2008) 016.

[11] Y. Imura, T. Okubo, S. Morita, and K. Okunishi, Snapshot Spectrum and critical phenomenon for two-dimensional classical spin systems, J. Phys. Soc. Jpn. **83**, 114002 (2014).

[12] H. Matsueda, Holographic entanglement entropy in Suzuki-Trotter decomposition of spin systems, Phys. Rev. E **85**, 031101 (2012).

[13] A. Pizzi and N. Y. Yao, Bipartite mutual information in classical many-body dynamics, Phys. Rev. B **110**, L020301 (2024).

[14] P. Davidson, *Turbulence: An Introduction for Scientists and Engineers*, 2nd ed. (Oxford University Press, Oxford, 2015).

[15] G. Falkovich, Y. Kadish, and N. Vladimirova, Multimode correlations and the entropy of turbulence in shell models, Phys. Rev. E **108**, 015103 (2023).

[16] T. Tanogami and R. Araki, Information-thermodynamic bound on information flow in turbulent cascade, Phys. Rev. Res. **6**, 013090 (2024).

[17] E. Kawamori, Identification of Langmuir wave turbulence-supercontinuum transition by application of von Neumann entropy, Phys. Plasmas **24**, 090701 (2017).

[18] G. Yatomi, M. Nakata, and M. Sasaki, Data-driven modal analysis of nonlinear quantities in turbulent plasmas using multi-field singular value decomposition, Plasma Phys. Controlled Fusion **65**, 095014 (2023).

[19] T. Kodahara, M. Sasaki, Y. Kawachi, Y. Jajima, T. Kobayashi, T. Yamada, H. Arakawa, and A. Fujisawa, Analysis of turbulence driven particle transport in PANTA by using multi-field singular value decomposition, Plasma Fusion Res. **18**, 1202036 (2023).

[20] A. Hasegawa and M. Wakatani, Plasma edge turbulence, Phys. Rev. Lett. **50**, 682 (1983).

[21] R. Numata, R. Ball, and R. L. Dewar, Bifurcation in electrostatic resistive drift wave turbulence, Phys. Plasmas **14**, 102312 (2007).

[22] Y.-C. Liang, M. R. Mazloff, I. Rosso, S.-W. Fang, and J.-Y. Yu, A multivariate empirical orthogonal function method to construct nitrate maps in the southern ocean, J. Atmos. Ocean. Technol. **35**, 1505 (2018).

[23] G. Yatomi and M. Nakata, Convergence study of multi-field singular value decomposition for turbulence fields, JSIAM Letters **16**, 109 (2024).

[24] P. H. Diamond, S.-I. Itoh, K. Itoh, and T. S. Hahm, Zonal flows in plasma—A review, Plasma Phys. Controlled Fusion **47**, R35 (2005).

[25] M. Nakata, T. H. Watanabe, H. Sugama, and W. Horton, Formation of coherent vortex streets and transport reduction in electron temperature gradient driven turbulence, Phys. Plasmas **17**, 042306 (2010).

[26] M. Nakata, T. H. Watanabe, H. Sugama, and W. Horton, Effects of parallel dynamics on vortex structures in electron temperature gradient driven turbulence, Phys. Plasmas **18**, 012303 (2011).

[27] M. Sasaki, T. Kobayashi, K. Itoh, N. Kasuya, Y. Kosuga, A. Fujisawa, and S.-I. Itoh, Spatio-temporal dynamics of turbulence trapped in geodesic acoustic modes, Phys. Plasmas **25**, 012316 (2018).

[28] H. Zhu, Y. Zhou, and I. Y. Dodin, On the structure of the drifton phase space and its relation to the Rayleigh-Kuo criterion of the zonal-flow stability, Phys. Plasmas **25**, 072121 (2018).

[29] B. N. Rogers, W. Dorland, and M. Kotschenreuther, Generation and stability of zonal flows in ion-temperature-gradient mode turbulence, Phys. Rev. Lett. **85**, 5336 (2000).

[30] H. Zhu, Y. Zhou, and I. Y. Dodin, Theory of the tertiary instability and the Dimits shift within a scalar model, J. Plasma Phys. **86**, 905860405 (2020).

[31] M. Nakata, T.-H. Watanabe, and H. Sugama, Nonlinear entropy transfer via zonal flows in gyrokinetic plasma turbulence, Phys. Plasmas **19**, 022303 (2012).

[32] T. Kobayashi, M. Yoshinuma, and K. Ida, Two-dimensional beam emission spectroscopy for hydrogen isotope negative neutral beam in large helical device, Plasma Phys. Controlled Fusion **62**, 125011 (2020).